H-SynEx: Using synthetic images and ultra-high resolution *ex vivo* MRI for hypothalamus subregion segmentation

Livia Rodrigues[a,b], Martina Bocchetta[c,d], Oula Puonti[a], Douglas Greve[a], Ana Carolina Londe[e], Marcondes França[e], Simone Appenzeller[e], Juan Eugenio Iglesias‡[a], Leticia Rittner‡[b]

[a]*Massachusetts General Hospital Harvard Medical School*
[b]*Universidade Estadual de Campinas, School of Electrical and Computer Engineering,*
[c]*Dementia Research Centre, Department of Neurodegenerative Disease, UCL Queen Square Institute of Neurology, University College London, London, United Kingdom,*
[d]*Centre for Cognitive and Clinical Neuroscience, Division of Psychology, Department of Life Sciences, College of Health, Medicine and Life Sciences, Brunel University London, United Kingdom,*
[e]*Universidade Estadual de Campinas - School of Medical Sciences,*

Abstract

- **Purpose** To develop a method for automated segmentation of hypothalamus subregions informed by ultra-high resolution *ex vivo* magnetic resonance images (MRI), which generalizes across MRI sequences and resolutions without retraining.

- **Materials and Methods** We trained our deep learning method, H-synEx, with synthetic images derived from label maps built from ultra-high resolution *ex vivo* MRI scans, which enables finer-grained manual segmentation when compared with $1mm$ isometric *in vivo* images. We validated this retrospective study using 1535 *in vivo* images from six datasets and six MRI sequences. The quantitative evaluation used the Dice Coefficient (DC) and Average Hausdorff distance (AVD). Statistical analysis compared hypothalamic subregion volumes in controls, Alzheimer's disease (AD), and behavioral variant frontotemporal dementia (bvFTD) subjects using the area under the curve (AUC) and Wilcoxon rank sum test.

‡Equal contribution

- **Results** H-SynEx can segment the hypothalamus across various MRI sequences, encompassing FLAIR sequences with significant slice spacing ($5mm$). Using hypothalamic volumes on T1w images to distinguish control from AD and bvFTD patients, we observed AUC values of 0.74 and 0.79 respectively. Additionally, AUC=0.66 was found for volume variation on FLAIR scans when comparing control and non-patients.

- **Conclusion** Our results show that H-SynEx successfully leverages information from ultra-high resolution scans to segment *in vivo* from different MRI sequences such as T1w, T2w, PD, qT1, FA, and FLAIR. We also found that our automated segmentation was able to discriminate controls versus patients on FLAIR images with $5mm$ spacing. H-SynEx is openly available at `https://github.com/liviamarodrigues/hsynex`.

---

1. Abreviation

DC = Dice Coefficient; AVD = Average Hausdorff Distance; AUC = area under the ROC curve; ROC = receiver operating characteristic; AD = Alzheimer's Disease, bvFTD = behavioral variant frontotemporal dementia; TIV = total intracranial volume

2. Summary

We propose H-SynEx, a segmentation method for the hypothalamus and its sub-regions trained on synthetic images derived from high-resolution *ex vivo* MRI, which is compatible with different sequences and resolutions of *in vivo* MRI.

3. Key Points

- The development of a fully automated segmentation method trained on synthetic images derived from *ex vivo* MRI label maps capable of identifying hypothalamic subregions across various MRI sequences and resolutions, including clinical acquisitions with large slice thickness;

- The usage of ultra-high resolution *ex vivo* images to build the label maps implies a more accurate model of the hypothalamus anatomy.

- H-SynEx outperforms other state-of-the-art methods in both patient-control comparisons conducted and is currently the only method capable of segmenting hypothalamic subregions on MRI sequences other than T1w and T2w.

4. Keywords

Hypothalamus segmentation, *ex vivo* MRI, domain randomization

5. Introduction

The hypothalamus is a small, cone-shaped, gray-matter structure located in the central part of the brain. It is composed of subnuclei containing the cell bodies of multiple neuron subtypes. Despite its small dimensions, the hypothalamus plays a significant role in controlling sleep, body temperature, appetite, and emotions, among other functions [1, 2]. While MRI is often employed to study brain structures *in vivo*, many analyses (e.g., volumetry) require manual segmentations that are challenging and time-consuming. For the hypothalamus, manual segmentation is particularly prone to high inter- and intra-rater variability due to its small size and low contrast with neighboring tissue. Even with the help of semi-automated methods, one segmentation can take up to 40 minutes to be completed [3], making large-scale studies impractical at most research sites. In the literature, several studies establish a connection between the whole hypothalamus and neurodegenerative diseases and other conditions using different MRI sequences [4, 5, 6, 7, 8]. , with some studies suggesting a differential involvement of the hypothalamic subregions across conditions [9]. However, these studies are limited to select sites and require specialists with neuroanatomical knowledge to perform manual annotation.

The use of semi-supervised models on medical images enhances the generalization of networks without necessarily increasing the quantity of annotated data [10, 11]. The use of synthetic images has also been a constant subject of study in the field, since it allows the construction of training datasets and flawless ground truths [12, 13]. Besides the synthetic approach, the usage of ultra-high resolution *ex vivo* MRI has proven to be beneficial in the segmentation of small structures such as the hippocampus, amygdala, and thalamus [14, 15, 16], as it permits a better visualization of their anatomical boundaries, leading to more accurate manual annotation.

Several methods have been proposed for the hypothalamus automated segmentation on T1w [17, 18, 19, 20, 21] and T2w images [19]. However, all these studies were conducted using manual segmentation of *in vivo* images with resolutions ranging between $0.8mm$ and $1mm$, which implies a higher partial volume effect and lower quality in manual segmentation when compared to delineations made on ultra-high-resolution *ex vivo* images. Besides, none of these methods can segment images at anisotropic resolution (often the case in clinical MRI) or in different sequences than the ones they were trained on.

3

In this article, we train a model using synthetic images derived from label maps built from ultra-high resolution *ex vivo* MRI. We hypothesize that employing synthetic images will help address various MRI contrasts while constructing the label maps from *ex vivo* images will provide more details of the hypothalamic anatomy, enhancing the automated segmentation quality. We aim to develop an automated method for hypothalamic subregion segmentation, which is robust against variations in MRI contrast and resolution of the input images - including retrospective clinical data, which often present large slice spacing.

6. Materials and Methods

6.1. Data

The FreeSurfer Maintenance (FSM) dataset [21], used during inference as a retrospective study, was approved by the Massachusetts General Hospital Internal Review Board for the protection of human subjects and all subjects gave written informed consent. All other retrospective datasets used for training and inference are openly available.

6.1.1. Training Data

The data used for training H-SynEx comprises synthetic images derived from label maps. These are built using a dataset consisting of 10 post mortem MRI acquisitions of brain hemispheres publicly available at the Distributed Archives for Neurophysiology Data Integration (DANDI Archive)[1] [22] (Fig. A.8), with resolution ranging from 120 to 150 μm and an equal distribution of 5 male and 5 female specimens. The age at the time of death ranges from 54 to 79 years, with an average of 66.4 $\pm$ 8.46 years. Five hypothalamic regions were manually labeled: anterior-superior, anterior-inferior, tuberal-superior, tuberal-inferior, and posterior. We also use labeled fornices to aid in training.

6.1.2. Test Data

Evaluation relies on 1535 *in vivo* images from 6 different datasets: FreeSurfer Maintenance (FSM) [21], MICLab-LNI Initiative (MiLI) [20], IXI [23], OASIS [24], ADNI [25] and NIFD [26] (See Appendix A.1).

---

[1]https://dandiarchive.org/dandiset/000026/draft/files?location=

4

6.2. Methods

6.2.1. Training

6.2.2. Data preprocessing

Initially, we resample the *ex vivo* images to $0.3x0.3x0.3mm$ isotropic. Then we create the label maps (Appendix A.2) by manually annotating the hypothalamus and utilizing automated segmentation for the remaining brain structures to establish context. Since the *ex vivo* images present only one hemisphere, we perform a mirroring step to generate a whole brain.Next, we crop the label maps around the hypothalamus into a region of interest of $200 \times 200 \times 200$, which corresponds to a field of view of $60 \times 60 \times 60mm$. To provide the network with detailed spatial context during training, we add three channels to the input with a positional encoding corresponding to the MNI coordinates, C_{crop}, of the voxels (Appendix B.1).

6.2.3. Synthetic Images Generation

The synthetic image generation is performed on the fly during training. At each iteration, one of the training label maps, L_{one}, is randomly selected. Then, we apply aggressive geometric augmentation that encompasses random crop, rotation, and elastic transformation on L_{one} and C_{crop}, ending up with $L_{\mathrm{trans}} [V \times 160 \times 160 \times 160]$ and $C_{\mathrm{trans}} [3 \times 160 \times 160 \times 160]$, respectively. V_{hyp} represents the total number of labels ($V = V_{\mathrm{brain}} + V_{\mathrm{hyp}}$). Next, we use the generative model proposed by Synth-Seg [13] based on Gaussian Mixture Models conditioned on L_{trans} using randomized parameters for contrast and resolution to create the final synthetic images $S [160 \times 160 \times 160]$ (Fig. 1). The target $T [V + 1 \times 160 \times 160 \times 160]$, derived from L_{trans}, is also created during this step. The additional channel on T designates the background. To assist training, we use an Euclidean distance map, $E[V + 1 \times 160 \times 160 \times 160]$ derived from T, which has been proven to be helpful in segmentation tasks [27]. E will be part of the loss function and is only employed during training, not being necessary during inference. The final input of the network, $I [4 \times 160 \times 160 \times 160]$, is the concatenation of S and C_{trans}.

6.2.4. Training architecture

Two distinct sub-models were trained separately (see Appendix B.2), one for the entire hypothalamus (M_{hyp}) and another specifically for its subregions (M_{sub}) (Fig. 2). Both M_{hyp} and M_{sub} are 3D-UNets [28, 29], however, in both cases, we added a skip connection between the input channels referring to C_{trans} and the final convolutional block to ensure that the original positional encoding is readily available at full-resolution also in the decoder. M_{hyp} receives I and E as input and outputs $O_{\mathrm{hyp}} [2 \times 160 \times 160 \times 160]$. The input of M_{sub} is defined as $I_{\mathrm{sub}} = I * O_{\mathrm{sub}}$.
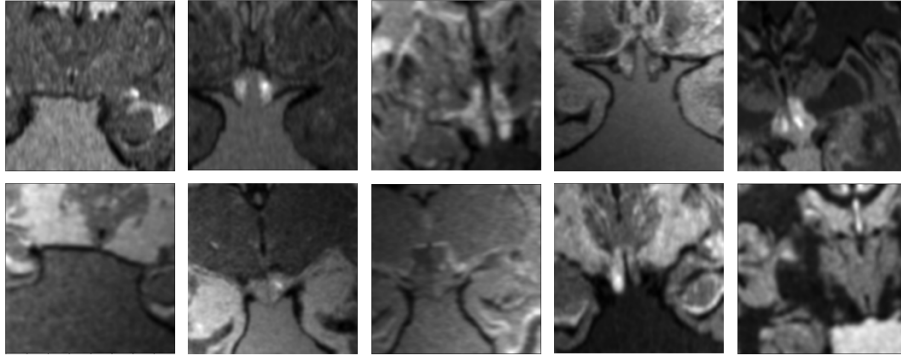
Figure 1: **Examples of coronal slices from 3D synthetic images used as input**: The images shown here are cropped around the hypothalamus. The use of aggressive data augmentation along random contrast values on the generative model results in large variability in the appearance of the input images.

While O_{hyp} is a 2-channel array representing the hypothalamus and its background, $O_{\text{sub}} [13 \times 160 \times 160 \times 160]$, the output of M_{sub}, is a 13-channel array encompassing the subregions, right and left fornices and background.

6.2.5. Loss

The loss function applied to M_{hyp} (1) is a combination of Dice Loss (DL) and Mean Square Error (MSE), while the loss function applied to M_{sub} (2) combines DL and Cross Entropý (CE):

$$L_{\text{hyp}} = \alpha * DL\left(T, T_{\text{pred}}\right) + \beta * \text{MSE}\left(E, E_{\text{pred}}\right) \tag{1}$$

$$L_{\text{sub}} = \alpha * DL\left(T, T_{\text{pred}}\right) + \beta * \text{CE}\left(T, T_{\text{pred}}\right) \tag{2}$$

After a few tests, α and β were chosen as 0.3 and 0.7, respectively, for both models.

6.2.6. Inference and Post processing

The first step of the inference (Fig. 3) is preprocessing, in which we find the MNI coordinates, C_{inf}, computed using a fast deep learning algorithm, EasyReg [30]. For M_{hyp}, the final input A_{inf} is the concatenation of inference image I_{inf} and C_{inf}. The input for M_{sub}, $A_{\text{inf\_sub}}$, is formed by the product of A_{inf}, the output of M_{hyp}, $O_{\text{hyp\_inf}}$, and the ventral diencephalon (VDC) label, which is derived from the whole brain segmentation produced by EasyReg [30]. The post-processing encompasses rescaling of the final segmentation to match the voxel size of I_{inf}, and the exclusion of voxels that belong to the third ventricle.
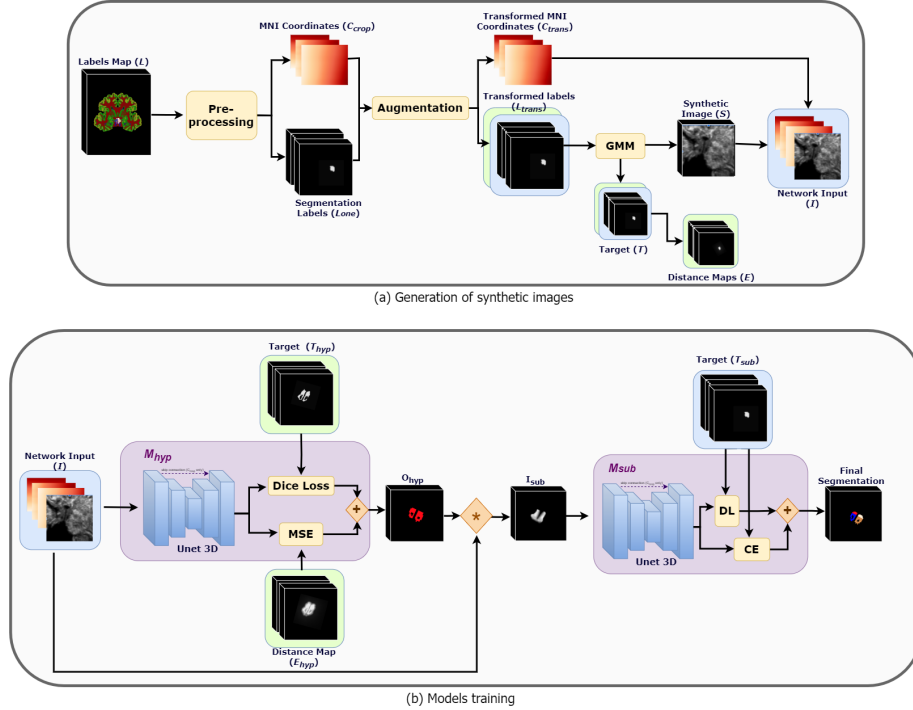
(a) Generation of synthetic images

(b) Models training

Figure 2: **Training Flowchart**: (a) Generation of synthetic images: The synthetic images S are generated using the label maps from the *ex vivo* images. (b) Models training: there are two training blocks, one focused on the entire hypothalamus and another specialized in subregion segmentation. The training of the two blocks is done subsequently. We first trained M_{hyp}, and later, M_{sub}. However, the output of Mhyp is used to assist the input creation of M_{sub}.

6.2.7. Method evaluation and Statistical Analysis

To evaluate H-SynEx, we conducted different experiments to assess its performance on different MRI sequences and compare it with other state-of-the-art methods. For quantitative evaluation, we utilized DC and AVD, as detailed in Appendix C - combined with Wilcoxon signed-rank tests to assess the statistical significance of differences. We also compared the ability of H-SynEx and competing methods to find statistical differences in the volume of hypothalamus subregions of controls and patients (AD and bvFTD). For this, we used Wilcoxon rank-sum test to assess the significance difference in medians between groups and Area Under the Curve (AUC) as a non-parametric version of effect sizes between groups. Finally, we use DeLong test to compare AUCs across methods operating on the same sample. All statistical tests were conducted with a confidence level of 95% ($p-value < 0.05$)
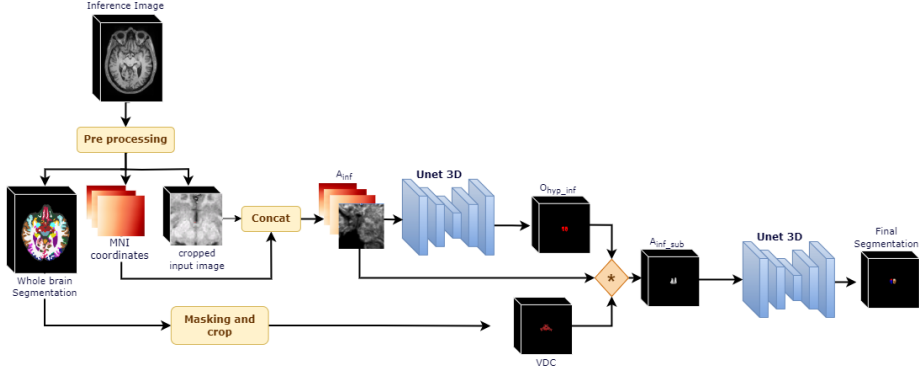
7

Figure 3: **Inference flowchart**: The inference image I_{inf} goes through a preprocessing step to find the input array A_{inf}. A_{inf} is then applied to M_{hyp}. Finally, using VDC, A_{inf} and $O_{\text{hyp\_inf}}$, we create the input for M_{sub} and find the final subregions segmentation.

7. Results

7.1. Experiment 1: Inter-rater metrics

One of the primary challenges in analyzing the results of our experiment is that each dataset used in testing has a distinct manual segmentation protocol, none of which aligns with the one employed in training H-SynEx. Therefore, our initial experiment aims to establish a baseline by comparing inter-rater metrics (AVD and DC) using distinct segmentation protocols on T1w images. We compare manual segmentations in 10 FSM images delineated by two different raters: the first uses the FSM protocol [21] while the second employs the protocol used during the label maps construction.

Given that Billot *et al* [18] is the only available method for subregion segmentation, we also compare its results with H-SynEx on 22 T1w images from FSM. H-SynEx outperforms Billot *et al* in almost every metric (Tab. 2). As we can see (Tabs. 1 and 2), the DC and AVD results among raters are comparable with the automated methods. It is important to emphasize that even among manual segmentations, the DC is lower than 0.66, which is expected due to the different segmentation protocols used and the small size of the hypothalamus subregions.

7.2. Experiment 2: Direct comparison with manual segmentation on different sequences

In this experiment, we aim to evaluate the ability of H-SynEx to properly segment the subregions of the hypothalamus in different MRI sequences. We employed five

8

Table 1: Inter-rater metrics (median) for 10 subjects from FSM

Metric / Subregion	DC	AVD
Anterior	0.63	0.41
Tuberal	0.66	0.43
Posterior	0.66	0.38

Table 2: AVD and DC (median) for H-SynEx and Billot *et al.* on different subregions for FSM dataset. Stars indicate the level of statistical significance (two-sided Wilcoxon rank-sum test) between both models (* $p < 0.05$, ** $p < 0.01$)

	Model / Subregion	H-SynEx	Billot *et al.*
AVD	Anterior	**0.54****	1.32
	Tuberal	**0.49****	0.66
	Posterior	**0.33****	0.52
DICE	Anterior	**0.53****	0.33
	Tuberal	**0.59**	**0.58**
	H-Posterior	**0.67****	0.55

different sequences from FSM - T1w, T2w, proton density (PD), fractional anisotropy (FA), and quantitative T1 (qT1)- and three from IXI -T1w, T2w, and PD. As the openly available methods exclusively operate on T1w images, a quantitative comparison of their metrics with H-SynEx was not possible in this experiment.

It is important to emphasize that the manual segmentation protocol used in both FSM and IXI is not the same as the one employed in the training dataset of H-SynEx. Besides, the small size of the hypothalamus may be related with the high variability of the metrics. To illustrate this point, we conducted a comparison of the volumes delineated by H-SynEx and manual segmentation in the FSM dataset (Figs. 4). We can see that both the posterior and anterior subregions, which show greater variability in the DC, are relatively smaller than the tuberal subregion. Furthermore, the variability in volumes across sequences and subregions appears to be less pronounced than the variability in metrics.

Observing the qualitative results (Fig. 6), we can assess that H-SynEx is capable of identifying the hypothalamus and its subregions across various sequences.
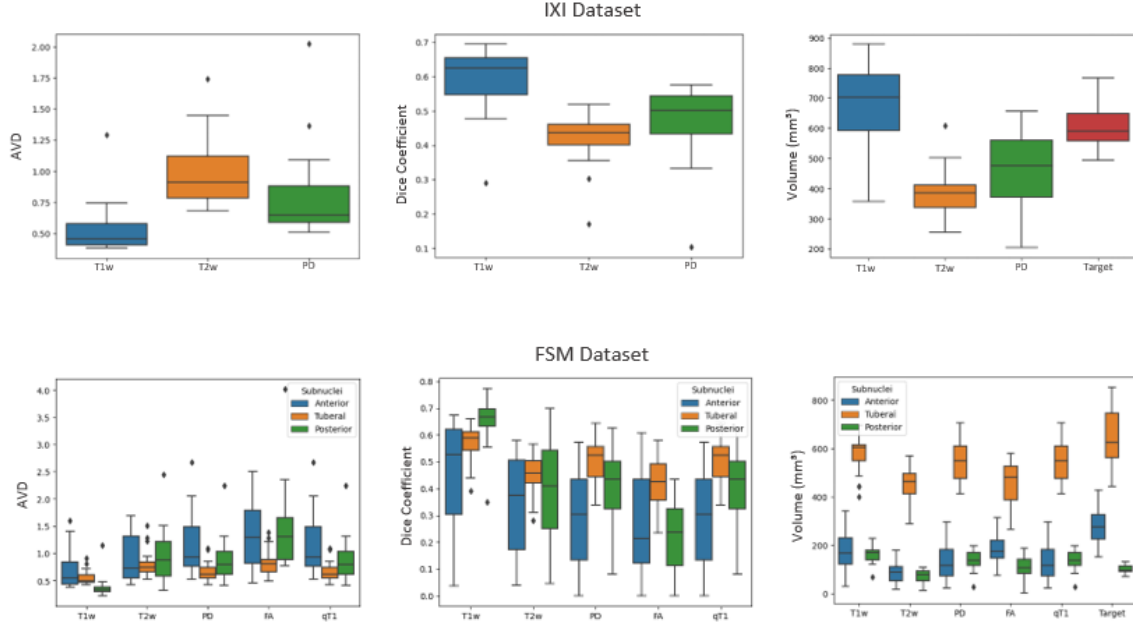
Figure 4: **Volume, DC, and AVD for H-SynEx across diverse sequences**. Top row: IXI dataset, which only presents the segmentation of the whole structure (excluding the mammillary bodies). Bottom row: FSM dataset, that contains the segmentation of the hypothalamus and its subregions.

7.3. Experiment 3: Comparing against other state-of-the-art methods

Here, we compare H-SynEx with other state-of-the-art models [18, 21] on T1w images from MiLI and FSM datasets for the whole hypothalamus. It is worth noting that the MiLI segmentation protocol does not include the mammillary bodies. Therefore, for this dataset, we excluded the posterior subregion from the results and computed the metrics. Given that the datasets have few subjects and we can not assess with high significance that the distribution is Gaussian, the statistical analyses were conducted considering non-parametric distributions. Observing AVD and DC (Tab. 3), H-SynEx outperforms Billot *et al* and returns similar results to ScLimbic on the former, despite not achieving the best performance on the latter. However, when dealing with small structures with complex boundaries, distance metrics are more suitable to compare different methods [31].

It is also important to highlight that the other methods were trained on *in vivo* T1w images, while H-SynEx was trained on synthetic images derived from *ex vivo* MRI. Therefore, even not presenting the best results in T1w images, H-SynEx

presents a bigger generalization ability.

Table 3: AVD and DC (median) for H-SynEx, ScLimbic [21] and Billot *et al.* [18] on different datasets (MiLI, IXI, OASIS, and FSM) for the entire hypothalamus (except MB). The symbols indicate statistical significance on a two-sided Wilcoxon rank-sum test using Bonferroni correction for $p < 0.05$: (*) Billot *vs* H-SynEx; ($\dagger$) ScLimbic *vs* H-SynEx; ($\ddagger$) Billot *vs* ScLimbic. Since ScLimbic was trained using the FSM dataset, we did not consider these results.

	Dataset / Model	MiLI	IXI	OASIS	FSM
AVD	Billot	0.46	$0.61^{*\ddagger}$	**0.47**	**0.40**
	ScLimbic	$\mathbf{0.39^{\dagger\ddagger}}$	**0.44**	**0.49**	-
	H-SynEx	0.45	**0.45**	**0.5**	**0.43**
DICE	Billot	0.66^{*}	0.6	$\mathbf{0.65^{*\ddagger}}$	**0.68**
	ScLimbic	$\mathbf{0.67^{\dagger\ddagger}}$	$\mathbf{0.64^{\dagger\ddagger}}$	0.59	-
	H-SynEx	0.63	0.62	0.58	**0.65**

7.4. Experiment 4: Application to group studies

In the literature, we can find studies that point to hypothalamic atrophy in both AD and bvFTD patients [9, 32]. Therefore, to evaluate the group studies, we compared the hypothalamic subregion volumes of patients and control groups from ADNI (AD subjects) and NIFD (bvFTD subjects). We normalized the volumes by dividing them by the total intracranial volume (TIV) provided by SynthSeg [13]. For comparative purposes, we conducted the analysis using Billot *et al.* and compared with H-SynEx through DeLong test [33].

H-SynEx achieved statistical significance ($p < 0.05$) in the Wilcoxon rank-sum test in all hypothalamic subregions when comparing AD vs. controls, while Billot *et al.* was unable to detect differences in the tuberal-inferior region (Tab. 4). Additionally, in some cases, we observed a higher area under the curve (AUC) in H-SynEx, along with a $p - value < 0.5$ for DeLong test, indicating the ability of H-SynEx to better discern differences between the two groups in this dataset. Regarding NIFD, the results were similar for both models, except for the tuberal-inferior region.

7.5. Experiment 5: Resilience to large slice spacing

In this experiment, we applied H-SynEx on FLAIR images from the ADNI dataset acquired with a slice spacing (and thickness) of $5mm$ in the axial plane. Here, we want to evaluate our method's capability to identify hypothalamic atrophy with

larger spacings, which are common in clinical MRI. Once no other method in the literature works with FLAIR images, we just compare the results from H-SynEx applied on FLAIR and T1w images. H-SynEx returns statistically significant results (Tab. 4) when comparing patient and control volumes normalized by TIV in all subregions, except for the posterior region. This may be explained by the $5mm$ spacing of the FLAIRs since it makes many images lack the MB, or limit it to just one slice of the image. For this reason, the lower AUC values in this subregion are expected. Finally, we plotted the correlation among T1w and FLAIR normalized volumes (Fig. 5) to investigate whether H-SynEx exhibits consistency among them. The anterior subregion displays a moderate correlation (r=0.40 and r=0.50, respectively), and tuberal subregions have strong correlations (r=0.79 and r=0.80, respectively), both for controls and AD subjects. As expected, the posterior correlation is weak in both cases (r=0.11 and r=0.22). These results support the hypothesis that the method can be used in challenging resolutions and still detect differences among groups.

Table 4: AUC Values for patients vs. controls for H-SynEx and Billot methods in ADNI and NIFD datasets. For ADNI dataset, we also analyze our method when applied to FLAIR images with spacing of $5mm$. Stars indicate the level of statistical significance (two-sided Wilcoxon rank-sum test) between both cohorts (* $p < 0.05$, ** $p < 0.01$). † indicates statistical significance on the DeLong test ($p < 0.05$) between H-SynEx and Billot methods. ‡ indicates statistical significance on the DeLong test ($p < 0.05$) between H-SynEx applied on T1-w and H-SynEx applied on Flairs.

Dataset	ADNI			NIFD	
Model ⟍ Subregion	H-SynEx Flair	H-SynEx T1w	Billot T1w	H-SynEx T1w	Billot T1w
Whole	0.66**‡	0.74**	0.65**†	0.79**	0.74**
a-sHyp	0.60**‡	0.69**	0.72**	0.76**	0.75**
a-iHyp	0.60**	0.64**	0.55*†	0.72**	0.62**
supTub	0.68**‡	0.60**	0.67**†	0.76**	0.76**
infTub	0.67**‡	0.73**	0.52†	0.74**	0.59*†
postHyp	0.52‡	0.72**	0.70**	0.7**	0.73**

8. Discussion

In this work, we introduced H-SynEx, a new automated segmentation method for the hypothalamus and its subregions based on synthetic images derived from high resolution *ex vivo* MRI. Because the hypothalamus is a small structure with low contrast compared to neighboring tissues, its manual segmentation is challenging,
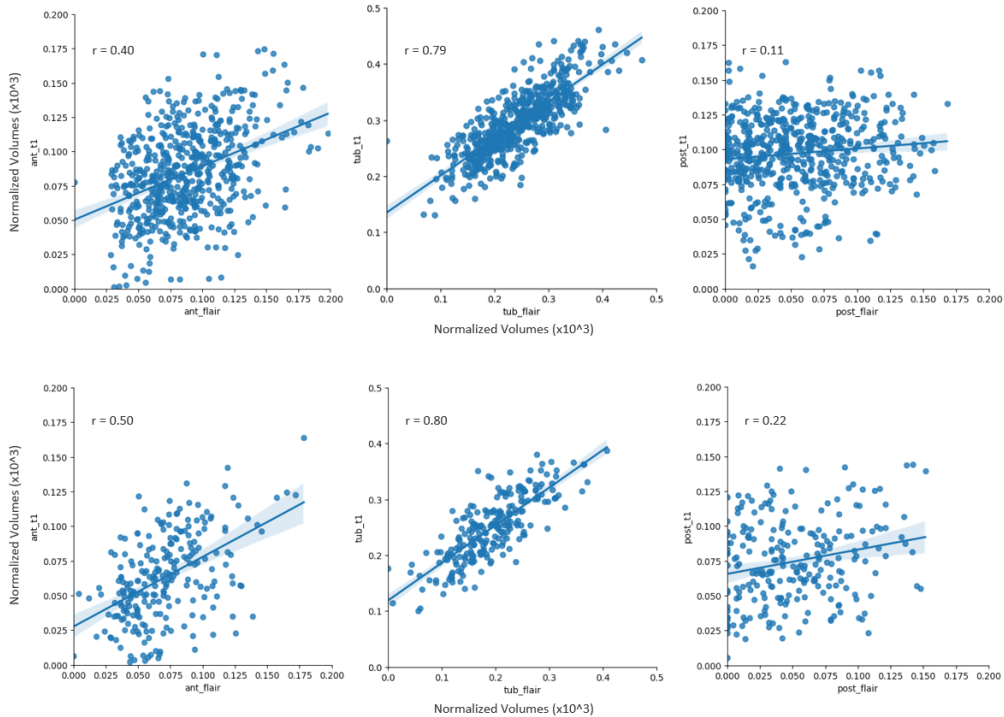
Figure 5: **Normalized volume correlation for FLAIRs *vs* T1w (ADNI Dataset) using H-SynEx segmentation**. Up: Control subjects; Down: AD patients. We can see that besides the posterior subregion, we can find a positive correlation between FLAIR and T1w normalized volumes.

and variable among and within raters. These characteristics extend across various MRI sequences. While other studies have utilized synthetic images [13] and *ex vivo* data [14] for developing segmentation methods applied to *in vivo* MRI, to the best of our knowledge, H-SynEx is the first to merge both techniques. Through this integration, we developed a method capable of effectively segmenting small structures, such as hypothalamus subregions, across various MRI sequences and resolutions, including FLAIRs with a spacing of $5mm$.

During the experiments, our major challenge was the disparity between training and inference segmentation protocols. To better understand the impact of these differences on our results, we compared the manual segmentation of two raters who employed distinct protocols on 10 T1w images from the FSM dataset. The DC values for all subregions in this experiment were below 0.7, indicating that quantitative metrics may be affected by the differences in the segmentation procedures. Since
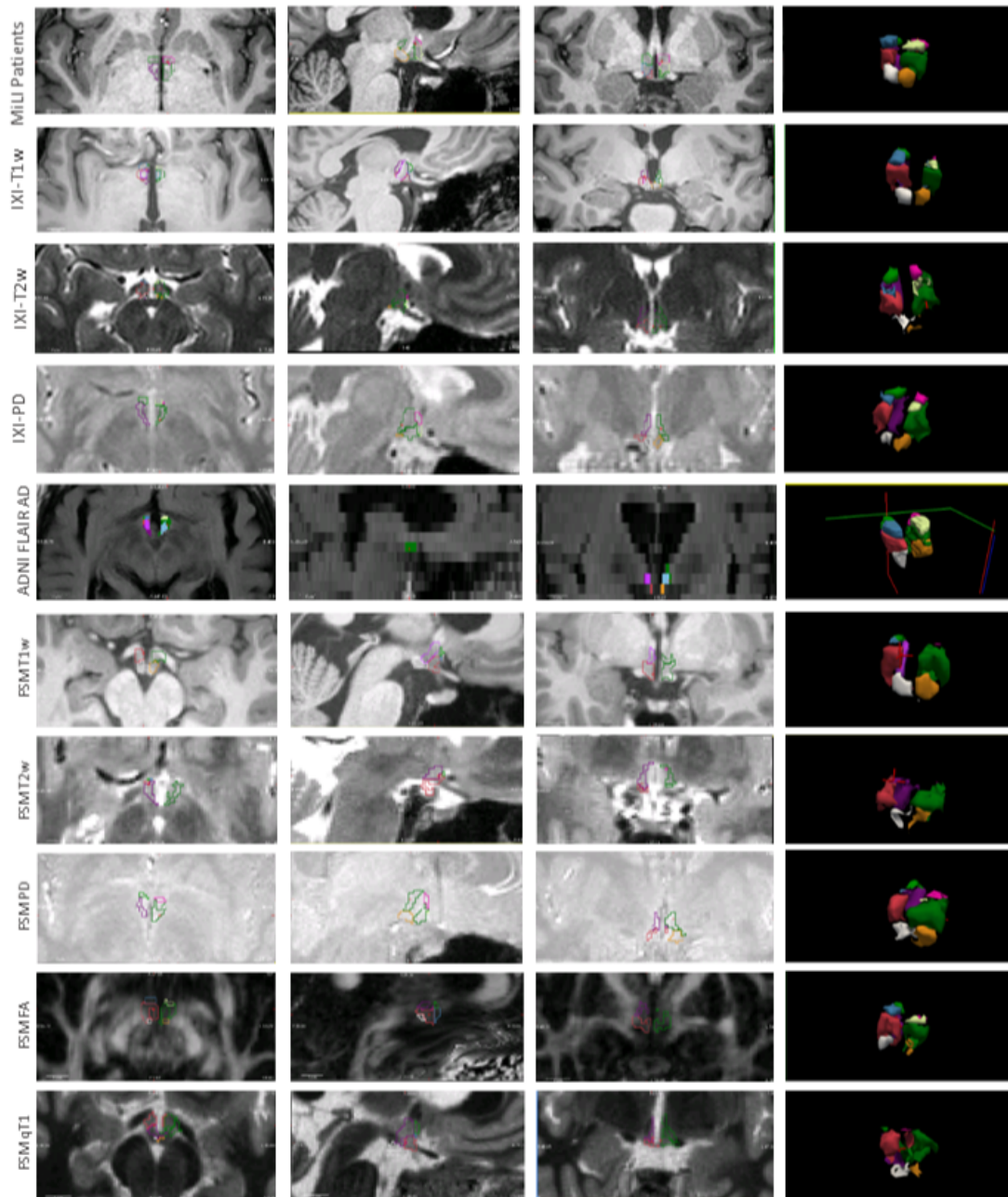
13

Figure 6: Qualitative results in different datasets, sequences, and resolutions for H-SynEx. Other methods, when applied to sequences different from T1w, return no results

14

DC is an overlap measure, it is sensitive to small structures, the reason why we also used the AVD as a quantitative metric. Still analyzing the subregions, we compared H-SynEx with Billot *et al*, the only publicly available method that segments hypothalamus subunits, on 22 T1w images from the FSM dataset. H-SynEx returned a better AVD in all subregions.

Through the experiments, we could also assess that H-SynEx is statistically comparable with other state-of-the-art hypothalamus segmentation methods when applied to T1w images. In this case, we compared the H-SynEx segmentation of the entire structure with Billot *et al* [18] and ScLimbic [21]. Given the small size of the hypothalamus, which may affect overlap measures, and its non-regular shaped borders, the AVD is more suitable to compare the results from different methods [31]. In this case, H-SynEx outperforms Billot *et al* [18] and obtains similar results to ScLimbic [21]. For DC, despite Billot *et al* [18] and ScLimbic [21] returning a better performance when compared with H-SynEx, none of the methods was able to obtain a DC bigger than 0.68, which conveys with the inter-rater analysis. For this experiment, it is worth noting that these comparisons were conducted solely on T1w images, as H-SynEx is the only available method capable of hypothalamic segmentation in other sequences. Also, it is important to emphasize that all other methods were exclusively trained on *in vivo* T1w images, not having to deal with domain gap.

When comparing volumes of the hypothalamus from patient and control groups on T1w images, we have confirmed that our method exhibits a statistically significant difference in all subregions in ADNI and NIFD datasets, with AUCs of 0.74 and 0.79 respectively, and $p - value < 0.05$ for the Wilcoxon signed-rank test in both cases. Notably, the AUC values reported to NIFD are higher than those found in ADNI. This behavior is expected since bvFTD patients tend to exhibit more pronounced hypothalamic atrophy than AD patients (10-12% volume loss in AD and 15-20% in bvFTD) [34]. Additionally, we determined that H-SynEx results differ statistically from Billot *et al* for the entire hypothalamus and in most subregions in the ADNI dataset, with a $p - value < 0.05$ for DeLong test. The method also demonstrates the ability to differentiate between patients and controls in challenging conditions, such as using FLAIRs with a spacing of $5mm$(AUC of 0.66 with $p - value < 0.05$ for Wilcoxon signed-rank test).

A limitation of the project is the difference in H-SynEx performance between T1w images and other sequences and the high variability of the metrics. However, besides the divergence in the manual segmentation protocols used for training and testing, in both IXI and FSM, we only have one label per subject. Therefore the manual segmentations were not influenced by different contrasts. Also, we could demonstrate that the smallest subregions (anterior and posterior) had the biggest

15

variability, especially in DC, an overlap measure known for being sensitive to small structures [31]. In the study groups, a decrease in the AUC is observed when analyzing FLAIR images and T1w images. The latter has a higher AUC, with a difference between the methods confirmed by the DeLong test ($p < 0.05$). Nevertheless, it is essential to remember that FLAIR images have a larger spacing between slices, which can also impact the results.

To the best of our knowledge, we have presented the first automated method for hypothalamic subregion segmentation capable of working across different *in vivo* MRI sequences and resolutions without retraining. By producing reliable and consistent segmentations, H-SynEx facilitates the analysis of the hypothalamus in various pre-existing datasets, whether in research or clinical settings. This contributes to an improved understanding of the roles played by the hypothalamus and its individual subregions in neurodegenerative diseases and other related conditions.

9. Acknowledgements

References

[1] C. Neudorfer, J. Germann, G. J. Elias, R. Gramer, A. Boutet, A. M. Lozano, A high-resolution in vivo magnetic resonance imaging atlas of the human hypothalamic region, Scientific Data 7 (1) (2020) 305.

[2] C. B. Saper, B. B. Lowell, The hypothalamus, Current Biology 24 (23) (2014) R1111–R1116.

[3] J. Wolff, S. Schindler, et al., A semi-automated algorithm for hypothalamus volumetry in 3 Tesla magnetic resonance images, Psychiatry Research: Neuroimaging 277 (2018) 45–51.

[4] M. Gorges, P. Vercruysse, et al., Hypothalamic atrophy is related to body mass index and age at onset in amyotrophic lateral sclerosis, Journal of Neurology, Neurosurgery & Psychiatry 88 (12) (2017) 1033–1041.

[5] J. Seong, J. Y. Kang, J. S. Sun, K. W. Kim, Hypothalamic inflammation and obesity: a mechanistic review, Archives of pharmacal research 42 (2019) 383–392.

[6] F. H. Wolfe, G. Auzias, et al., Focal atrophy of the hypothalamus associated with third ventricle enlargement in autism spectrum disorder, Neuroreport 26 (17) (2015) 1017–1022.

[7] R. Piyush, S. Ramakrishnan, Analysis of sub-anatomic volume changes in Alzheimer brain using diffusion tensor imaging, in: 2014 40th Annual Northeast Bioengineering Conference (NEBEC), IEEE, 2014, pp. 1–2.

[8] E. A. Schur, S. J. Melhorn, S.-K. Oh, J. M. Lacy, K. E. Berkseth, S. J. Guyenet, J. A. Sonnen, V. Tyagi, M. Rosalynn, B. De Leon, et al., Radiologic evidence that hypothalamic gliosis is associated with obesity and insulin resistance in humans, Obesity 23 (11) (2015) 2142–2148.

[9] M. Bocchetta, E. Gordon, et al., Detailed volumetric analysis of the hypothalamus in behavioral variant frontotemporal dementia, Journal of Neurology 262 (2015) 2635–2642.

[10] A. R. Fayjie, R. Dutta, P. Kashyap, U. R. Kumar, P. Vandewalle, Semi-supervised adversarial few-shot learning for medical image segmentation (2022).

[11] G. Bortsova, F. Dubost, L. Hogeweg, I. Katramados, M. De Bruijne, Semi-supervised medical image segmentation via learning consistency under transformations, in: Medical Image Computing and Computer Assisted Intervention–MICCAI 2019: 22nd International Conference, Shenzhen, China, October 13–17, 2019, Proceedings, Part VI 22, Springer, 2019, pp. 810–818.

[12] V. Thambawita, P. Salehi, S. A. Sheshkal, S. A. Hicks, H. L. Hammer, S. Parasa, T. d. Lange, P. Halvorsen, M. A. Riegler, Singan-seg: Synthetic training data generation for medical image segmentation, PloS one 17 (5) (2022) e0267976.

[13] B. Billot, D. N. Greve, O. Puonti, A. Thielscher, K. Van Leemput, B. Fischl, A. V. Dalca, J. E. Iglesias, et al., Synthseg: Segmentation of brain mri scans of any contrast and resolution without retraining, Medical image analysis 86 (2023) 102789.

[14] J. E. Iglesias, J. C. Augustinack, K. Nguyen, C. M. Player, A. Player, M. Wright, N. Roy, M. P. Frosch, A. C. McKee, L. L. Wald, et al., A computational atlas of

the hippocampal formation using ex vivo, ultra-high resolution mri: application to adaptive segmentation of in vivo mri, Neuroimage 115 (2015) 117–137.

[15] Z. M. Saygin, D. Kliemann, J. E. Iglesias, A. J. van der Kouwe, E. Boyd, M. Reuter, A. Stevens, K. Van Leemput, A. McKee, M. P. Frosch, et al., High-resolution magnetic resonance imaging reveals nuclei of the human amygdala: manual segmentation to automatic atlas, Neuroimage 155 (2017) 370–382.

[16] J. E. Iglesias, R. Insausti, G. Lerma-Usabiaga, M. Bocchetta, K. Van Leemput, D. N. Greve, A. Van der Kouwe, B. Fischl, C. Caballero-Gaudes, P. M. Paz-Alonso, et al., A probabilistic atlas of the human thalamic nuclei combining ex vivo mri and histology, Neuroimage 183 (2018) 314–326.

[17] L. Rodrigues, T. Rezende, et al., Hypothalamus fully automatic segmentation from MR images using a U-Net based architecture, in: 15th SIPAIM, Vol. 11330, International Society for Optics and Photonics, 2020, p. 113300J.

[18] B. Billot, M. Bocchetta, et al., Automated segmentation of the hypothalamus and associated subunits in brain MRI, NeuroImage 223 (2020) 117287.

[19] S. Estrada, D. Kügler, E. Bahrami, P. Xu, D. Mousa, M. Breteler, N. A. Aziz, M. Reuter, Fastsurfer-hypvinn: Automated sub-segmentation of the hypothalamus and adjacent structures on high-resolutional brain mri, arXiv preprint arXiv:2308.12736 (2023).

[20] L. Rodrigues, T. J. R. Rezende, G. Wertheimer, Y. Santos, M. França, L. Rittner, A benchmark for hypothalamus segmentation on t1-weighted mr images, NeuroImage 264 (2022) 119741.

[21] D. N. Greve, B. Billot, D. Cordero, A. Hoopes, M. Hoffmann, A. V. Dalca, B. Fischl, J. E. Iglesias, J. C. Augustinack, A deep learning toolbox for automatic segmentation of subcortical limbic structures from mri images, Neuroimage 244 (2021) 118610.

[22] Distributed archives for neurophysiology data integrationdoi:https://doi.org/10.5281/zenodo.7041535.

[23] IXI Dataset, https://brain-development.org/ixi-dataset/, accessed: 2023-11-29.

[24] P. J. LaMontagne, T. L. Benzinger, J. C. Morris, S. Keefe, R. Hornbeck, C. Xiong, E. Grant, J. Hassenstab, K. Moulder, A. Vlassenko, et al., OASIS-3: longitudinal neuroimaging, clinical, and cognitive dataset for normal aging and Alzheimer disease, MedRxiv (2019).

[25] S. G. Mueller, M. W. Weiner, L. J. Thal, R. C. Petersen, C. Jack, W. Jagust, J. Q. Trojanowski, A. W. Toga, L. Beckett, The alzheimer's disease neuroimaging initiative, Neuroimaging Clinics 15 (4) (2005) 869–877.

[26] NIFD Dataset, https://ida.loni.usc.edu/collaboration/access/appLicense.jsp, accessed: 2023-11-29.

[27] X. Liu, L. Yang, J. Chen, S. Yu, K. Li, Region-to-boundary deep learning model with multi-scale feature fusion for medical image segmentation, Biomedical Signal Processing and Control 71 (2022) 103165.

[28] A. Wolny, L. Cerrone, A. Vijayan, R. Tofanelli, A. V. Barro, M. Louveaux, C. Wenzl, S. Strauss, D. Wilson-Sánchez, R. Lymbouridou, S. S. Steigleder, C. Pape, A. Bailoni, S. Duran-Nebreda, G. W. Bassel, J. U. Lohmann, M. Tsiantis, F. A. Hamprecht, K. Schneitz, A. Maizel, A. Kreshuk, Accurate and versatile 3d segmentation of plant tissues at cellular resolution, eLife 9 (2020) e57613. doi:10.7554/eLife.57613.
URL https://doi.org/10.7554/eLife.57613

[29] Ö. Çiçek, A. Abdulkadir, S. S. Lienkamp, T. Brox, O. Ronneberger, 3d u-net: learning dense volumetric segmentation from sparse annotation, in: Medical Image Computing and Computer-Assisted Intervention–MICCAI 2016: 19th International Conference, Athens, Greece, October 17-21, 2016, Proceedings, Part II 19, Springer, 2016, pp. 424–432.

[30] J. E. Iglesias, Easyreg: A ready-to-use deep learning tool for symmetric affine and nonlinear brain mri registration (2023).

[31] A. A. Taha, A. Hanbury, Metrics for evaluating 3D medical image segmentation: analysis, selection, and tool, BMC medical imaging 15 (1) (2015) 1–28.

[32] A. Tao, Z. Myslinski, Y. Pan, C. Iadecola, J. Dyke, G. Chiang, M. Ishii, Hypothalamic atrophy in alzheimer's disease (1819) (2021).

[33] E. R. DeLong, D. M. DeLong, D. L. Clarke-Pearson, Comparing the areas under two or more correlated receiver operating characteristic curves: a nonparametric approach, Biometrics (1988) 837–845.

[34] P. Vercruysse, D. Vieau, et al., Hypothalamic alterations in neurodegenerative diseases and their relation to abnormal energy metabolism, Front.Mol. Neurosci. 11 (2018) 2.

Appendix A. Data

Appendix A.1. Inference Datasets

The inference was done using *in vivo* data from 6 different datasets:

- **FreeSurfer Maintenance (FSM)** [21]: Composed of 29 subjects from which 7 were used for validation and 22 for testing. For each subject, we have T1w, T2w, PD, FA, and qT1 acquisitions (Fig. A.7). FSM contains manual labeling for the whole hypothalamus done on qT1 images.

- **MiLI** [20]: The MICLab-LNI Initiative is a dataset that contains manual and automated segmentations of the whole hypothalamus, however it does not contain the segmentation for the subregions. It is composed of subjects from different open datasets (MiLI, OASIS [24], IXI [23]). We only used the manually segmented T1w images, totaling 55 from MiLI (control and ataxia patients), 23 from OASIS, and 19 from IXI. In the case of IXI, as the dataset also encompasses T2w and proton density (PD) acquisitions, we incorporated these modalities in our experiments.

- **ADNI** [25]: We used a total of 572 controls (280 male and 292 female with average age of 75.5 ± 6.4 and 73.6 ± 6.01, respectively) and 271 Alzheimer's disease (AD) patients (143 male and 98 female with average age of 75.34 ± 7.6 and 73.8 ± 7.6, respectively) for both T1w and FLAIR modalities. ADNI dataset does not have manual segmentation of the hypothalamus.

- **NIFD** [26]: From the Neuroimaging in Frontotemporal Dementia dataset, we used 111 controls (49 male and 62 female with average age of 61.8 ± 7.4 and 63.4 ± 7.8, respectively) against 74 behavioral variant frontotemporal dementia (bvFTD) patients (51 male and 23 female with average age of 61.16 ± 5.8 and 62.4 ± 7.7, respectively). NIFD dataset does not have manual segmentation of the hypothalamus.

Appendix A.2. Label maps creation

The primary challenge associated with the use of *ex vivo* images relies on the fact that the hypothalamus is situated in the center of the brain and the images comprise only one hemisphere. Consequently, part of the contextual information about its surrounding tissue is lost. However, the employment of these images is justified due to their high resolution, ranging from 120 to 150 μm, which facilitates
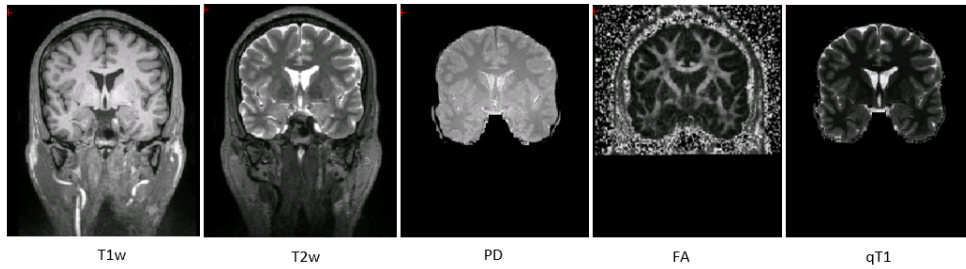
Figure A.7: Example of different modalities (FSM dataset)

the visualization of the hypothalamus landmarks, allowing a more precise manual segmentation.

The final training data is comprised of synthetic images derived from label maps created from the *ex vivo* images (Fig. A.8).
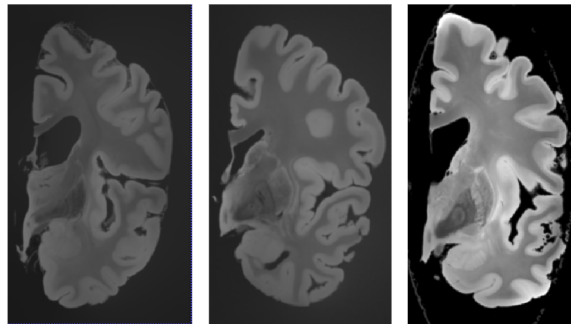

Figure A.8: Example of *ex vivo* images used to create the label maps

The main steps for label map creation are:

- *Image preprocessing*: At first, a sequence of preprocessing steps are executed on the original *ex vivo* images: image reorientation to conform to positive RAS standards, elimination of all non-brain voxels, voxel resampling to 0.3 mm^3, and bias field correction.

- *Hypothalamus manual segmentation*: Using the preprocessed images, we manually segmented the hypothalamus and its subnuclei of the 10 *ex vivo* images:

    - Right Anterior-Inferior

22

- Right Anterior-Superior
- Right Tuberal-Inferior
- Right Tuberal-Superior
- Right Posterior
- Left Anterior-Inferior
- Left Anterior-Superior
- Left Tuberal-Inferior
- Left Tuberal-Superior
- Left Anterior-Inferior

- *Whole brain automated segmentation*: Although the segmentation of the hypothalamus was performed manually, we did not require precise segmentation for other brain structures, as all we needed was the context around the hypothalamus. Therefore, we conducted a bias field correction on the *ex vivo* images and ran a k-means algorithm with values of k ranging from 4 to 9. Finally, we merged the automated and manual segmentation into one image.

- *Image mirroring*: The *ex vivo* images were acquired using only one hemisphere of the brain. Given that the hypothalamus is situated in the brain's center, there was a lack of contextual information regarding its surroundings. To address this concern, we mirrored the images to generate a complete brain (Fig. A.9).
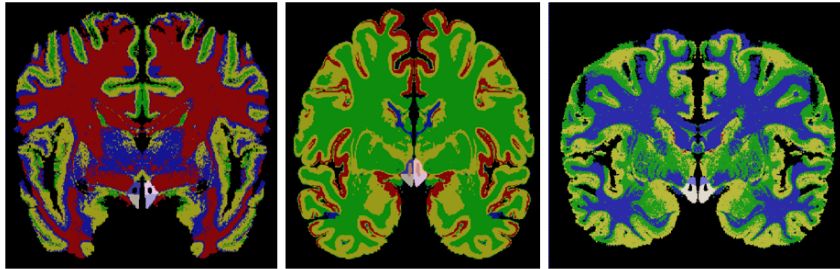

Figure A.9: Example of label maps

23

Appendix B. Method

Appendix B.1. Pre Processing

- Registration: Using the label maps $L[D \times H \times W]$ as a starting point, we generate a Gaussian image $G[D \times H \times W]$ that simulates a T1w MRI. Subsequently, we registered G to the MNI space using NiftiReg and obtained the MNI coordinates $C[3 \times D \times H \times W]$ of the registered image. It is important to emphasize that L remains unregistered.

- Crop: By applying the transformation matrix from the previous step on the MNI coordinates of the hypothalamus, we can find its voxel coordinates on L. This allows us to crop L and C around the hypothalamus, resulting in two standardized arrays, $L_{\mathrm{crop}}[200 \times 200 \times 200]$ and $C_{\mathrm{crop}}[3 \times 200 \times 200 \times 200]$.

- One-hot array: We convert L_{crop} into a one-hot array $L_{\mathrm{one}}[V \times 200 \times 200 \times 200]$, being V the number of labels presented on L_{crop}. V varies according to the number of labels V_{brain} employed on the whole brain segmentation (Section Appendix A.2) and the labels V_{hyp} used for the hypothalamus. Therefore, $V = V_{\mathrm{brain}} + V_{\mathrm{hyp}}$.

Appendix B.2. Training details

During the method development, we first trained M_{hyp}, which is focused on the whole structure. Then, we used the trained weights to help find an input for M_{sub}. For both models, we used Adam optimizer with a learning rate of $5*10^{-5}$, and a batch size of 32. We did not apply a validation set for M_{hyp} using the last checkpoint after approximately 40000 training steps. However, on M_{sub}, we used five acquisitions of 7 subjects from FSM, resulting 35 images as a validation set. We set an early stop criteria based on the dice coefficient of the validation set. For this, we defined the stopping criteria as $\delta_{min} = 0.001$ or patience of 200 epochs. The network trained for approximately 28000 steps and stopped. Both UNet modules are composed by an encoder of 5 levels with 24, 48, 96, 192, and 384 feature maps. Each convolutional block is composed of a GroupNorm3D layer, convolution, and activation function (ReLU).

Appendix B.3. Inference and Post-processing

The first step of the inference is preprocessing. First, we need to find the MNI coordinates C_{inf} for the inference image $I_{\mathrm{inf}}[D \times H \times W]$. Differently from the training step, here we do not need to find G. Hence, we simply employ EasyReg [30]. Both I_{inf} and C_{inf} are then concatenated, rescaled to a voxel resolution of $0.3mm^3$

to follow L resolution (Section Appendix A.2), and cropped around the hypothalamus using the same strategy we employed on the training images. The resulting array $A_{\text{inf}}[4, 160 \times 160 \times 160]$, is the inference input. Then, A_{inf} is applied to the first segmentation block M_{hyp}, resulting on $O_{\text{hyp\_inf}}$. The input for M_{sub}, $A_{\text{inf\_sub}}$ is formed by the product of A_{inf}, $O_{\text{hyp\_inf}}$ and the ventral diencephalon (VDC) label, $\text{VDC}[160 \times 160 \times 160]$, which is derived from the whole brain segmentation produced by EasyReg. The inclusion of the ventral-DC label is justified as it helps reduce false positives within the anterior subregion. The post-processing phase comprises two sequential steps: the rescaling of the final segmentation to match the voxel size of I_{inf}, and the exclusion of voxels that belong to the third ventricle by using the whole brain segmentation obtained from EasyReg.

Appendix C. Evaluation Metrics

We employed two distinct metrics to conduct a quantitative analysis of the results: the Dice coefficient (DC) and the average Hausdorff distance (AVD). Our selection of these metrics was influenced by the specific characteristics of the hypothalamus (a small structure with low contrast) and the established usage of these metrics in the scientific literature.

- **Dice Coefficient:**

  The DC is an overlap measure defined as follows:

$$DC = \frac{2 * |M \cap A|}{|M| + |A|} \tag{C.1}$$

  DC is sensitive to small segmentation and does not identify boundary errors. However, it can be used as a measure of reproducibility and is widely used for medical imaging segmentation analysis, being the most used metric in the medical imaging segmentation field. DC results may be in the [0,1] range, where 1 a perfect DC

- **Average Hausdorff Distance**:

  AVD is the averaged Hausdorff Distance over all points.

$$AVD(A, M) = max(d(A, M), d(M, A)) \tag{C.2}$$

  where:

$$d(A, M) = \frac{1}{N} \sum_{a \epsilon A} \min_{m \epsilon M} \|a - m\| \qquad \text{(C.3)}$$

It is a spatial distance metric that unlike DC, can find boundary errors which can occur owing to low contrast of the *in vivo* images. Moreover, it demonstrates greater robustness in the context of small structures, such as the hypothalamus. The smaller the AVD between manual and automated segmentation, the better the automated segmentation.